DOI: 10.1007/s00267-001-2645-8

Detection of Coastal Saline Land Uses with Multi-Temporal Landsat Images in Shangyu City, China

ZHOU SHI*
RENCHAO WANG
MING XIANG HUANG
Institute of Agricultural Remote Sensing and Information System
Huajiachi Campus, Zhejiang University,
Hangzhou, China 310029

DIRK LANDGRAF
Institute of Soil Science
Technical University of Dresden
Tharandt, Germany

ABSTRACT / Many coastal regions in China are confronted with pressing problems of scarce land resources and heavy population. Over the past 30 years, considerable parts of coastal tidelands have been enclosed and reclaimed for agricultural land uses. To assess, plan, and implement large-scale reclamation programs, up-to-date and reliable information concerning the nature, areal extent, and physical and chemical characteristics of coastal saline lands is essential. This paper reports a remote sensing approach to detecting coastal saline land uses in Shangyu City, China, by using multi-temporal Landsat images. First, with the aid of resolution-sharpened Landsat-7 ETM+ images and their enhanced linear features, a visual interpretation is applied to extract individual dikes. Based on time series images and local government records, a spatial zoning procedure is then used to define six sub-zones with different historical years of reclamation. It shows that a total of 15,668 ha of coastal saline lands were enclosed and reclaimed from 1969 to 1996. Second, a modified land-use classification system for the study area is prescribed, and both unsupervised and supervised classifiers are performed for land-use classifications of grouped sub-zones. Information obtained from the spatial zoning, Tasseled Cap transformation and Normalized Difference Vegetation Index, is also utilized to facilitate the supervised classification process. Finally, a detailed land-use map is produced, with an overall classification accuracy of 77.8%. Results show that dominant agricultural land uses of sub-zones are changed with historical reclamation years, from saline lands with wildgrass (very recently reclaimed) to aqua-farm ponds, to cotton fields, and to paddy fields and orchards (very early reclaimed). This transform process is primarily affected by soil salinities, and according to a soil survey an electrical conductivity of saturation extract decreased from 7.3 ds/m in the saline land reclaimed in 1996 to below 2 ds/m in the land reclaimed before 1969. The study concludes that multi-temporal remotely sensed images are important and effective data sources for monitoring the rapid changes of coastal land uses.

Many costal regions in China are confronted with challenging problems of limited land resources and increasing population. For example, in Zhejiang Province arable land per capita is 0.037 ha only, less than 50% of the national average. During the past 30 years, a total of 400,000 ha tidelands (equivalent to 4.1% of the total area of Zhejiang Province) have been enclosed for agricultural land uses and urbanization buffer zones under a series of reclamation programs. In Shangyu City of Zhejiang Province, approximately 17,000 ha coastal saline lands have been reclaimed, producing a half of cottons, fruits, and aquatic products of the city.

To access, plan, and implement large-scale reclamation programs, timely and reliable spatial information on the nature, area extent, and physical and chemical characteristics of coastal saline lands is important. Coastal land uses with different levels of reclamation intensity and soil salinities need to be closely monitored at an appropriate time interval. The recent development of geospatial technologies, such as remote sensing (RS) and geographic information systems (GIS), can play an important role in such tasks of coastal management (Mumby and others 1995). Modern remote sensing approaches have advantages over conventional field survey techniques, which are laborious and costly. Time series remotely sensed images with a medium spatial resolution are ideal data sources for mapping coastal land uses and monitoring their changes for a large area. For example, the Landsat-7 Enhanced Thematic Mapper Plus (ETM+) sensor extends capabilities of the Landsat TM by providing a 15 m resolution panchromatic band, and by allowing accurate (±5%) radiometric calibration on-board. As a supplement to previous Landsat data, this new image source

KEY WORDS: Coastal land-use; Saline soil; Multitemporal; Remote sensing; Classification

*Author to whom correspondence should be addressed; *email:* shizhou@zju.edu.cn

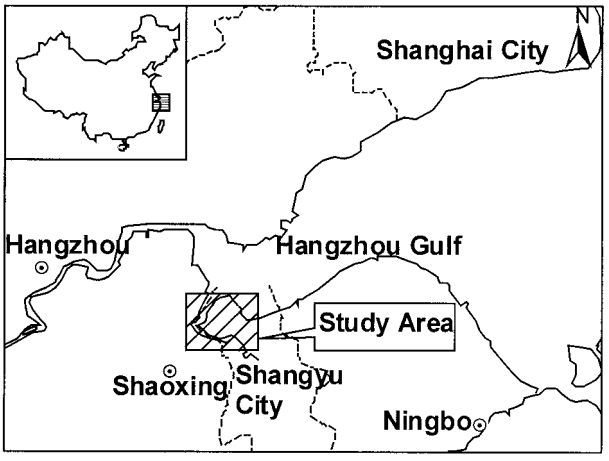

Figure 1. Location of the study area.

(available since 1999) would widen applications of remote sensing in coastal land uses and other natural resources management.

While remote sensing approaches have been used to map different agricultural land uses (Hill and Megier 1988, Wheeler and others 1988, Salem and others 1995, El-Khattib and others 1996), very few studies apply multi-temporal Landsat images to monitor agricultural land-use changes (Hill and Megier 1989, Pax-Lenney and Woodcock 1997, Goetz and others 2000). Furthermore, previous studies mainly focused on inland salt-effected lands (Dwivedi and Rao 1992, Kalra and Joshi 1996, Peng 1998), and little work has been reported on coastal agricultural land uses that have been reclaimed for many decades. This paper uses multi-temporal Landsat images to classify coastal land uses, primarily agricultural land uses, and to monitor their changes in relation to soil salinity levels. Two specific objectives are: (1) to extract dykes built over past 30 years and estimate areal changes of reclaimed coastal lands with multi-temporal Landsat MSS, TM, and ETM+ images; and (2) to classify current coastal land uses and monitor their changes in various reclaimed sub-zones, using multi-seasonal TM and ETM+ images.

Study Area and Data Sources

The study area is a northern part of Shangyu City, and situated at the south shore of Hangzhou Gulf (Figure 1). It covers approximately 26,061 ha, bounded by latitudes 30°04′00″N and 30°13′47″N, and longitudes 120°38′32″E and 120°51′53″E. The area belongs to a subtropical region with evergreen broad-leaved vegetation, an average annual temperature of 16.5°C, and an average annual precipitation of 1300 mm. Main soils are formed by modern marine and fluviatile deposit matters. Soil textures are light loam or sandy loam, with high concentrations of Na- and Mg-salts (>1%). A soil electrical conductivity of saturation extract, which is a very important index of assessing soil salinity (Rhoades and Miyamoto 1990), ranges from less than 2 ds/m (1m depth profile) in early reclaimed saline soils to 7.3 ds/m in recently reclaimed saline soils.

Table 1. A list of Landsat images

Date	Landsat images
29/10/1973	MSS, RGB 4/5/7 Photo
5/7/1978	MSS, RGB 4/5/7 Photo
4/8/1984	TM, RGB 2/3/4 Photo
8/3/1990	TM, RGB 3/4/7 Photo
23/7/1991	TM image
5/11/1994	TM image
1/10/1999	TM image
3/11/1999	ETM+ image
4/5/2000	ETM+ image

A series of Landsat images from 1973 to 2000, including Landsat MSS, TM, and ETM+ images, were acquired (Table 1). Ground reference data of various land-use types for image interpretation were collected by field investigations. During samplings of typical plants and saline soils at different sites, a portable GPS device was employed to determine sample locations. A topographical map with the scale of 1:10,000, from the Bureau of Surveying and Mapping of Zhejiang Province, was also available. Imagine 8.4 (an image processing program) and Arc/Info 8.0.2 (a vector-based GIS program) were used to analyze remotely sensed images and GIS data layers.

Methodology

An image analysis methodology employed in the study is shown in Figure 2, including three major steps: (1) image preprocessing, (2) dyke extraction and spatial zoning, and (3) image classification of different land uses.

Image Preprocessing

In order to geometrically correct digital Landsat images, a third order polynomial method was applied. Ten distinguishable ground control points (e.g., intersections of dykes and/or roads) were selected from the topographical map. After correction, a mean squared error (MSE) was 9.8 m.

Landsat 7 ETM+ images include a panchromatic band with a spatial resolution of 15 m and six multi-

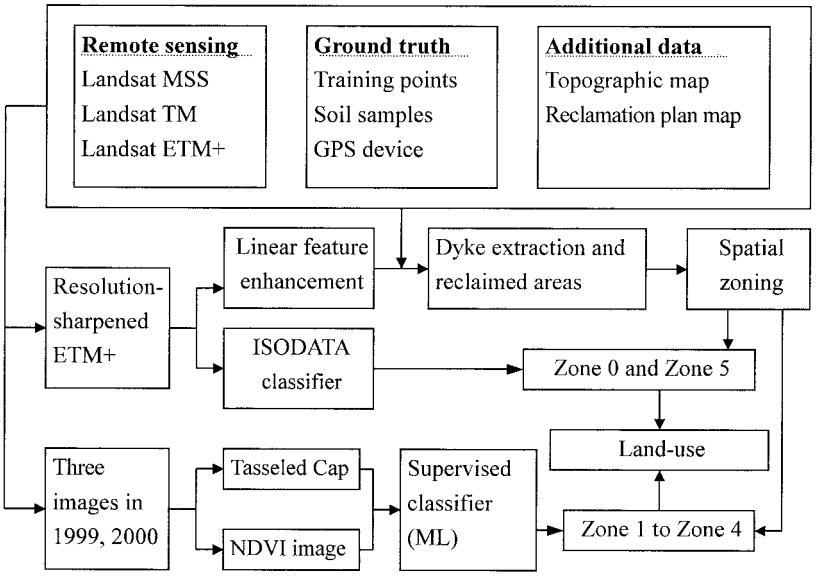

Figure 2. Methodology of land-use classification.

spectral bands with a spatial resolution of 30 m. To fully use the best characteristics of both higher resolution and spectral information, the above two types of images can be fused to derive new multispectral images yet with a spatial resolution of 15 m. In this study, a procedure called the forward-reverse principal components transformation (ERADS 1999) was implemented to achieve image mergers. Resolution-sharpened images were then produced, ready for the use of next processing steps.

Dyke Extraction and Spatial Zoning

A set of resolution-sharpened multispectral images derived from the 4 May 2000 ETM+ image was utilized to assist dyke features. First, several linear enhancement methods, including edge filter and texture analysis, were tested (ERADS 1999). It was indicated that the texture analysis of variance operator with a 5 pixel × 5 pixel window produced the best discrimination of linear features. Then, a visual interpretation was followed to extract individual dykes. With the aid of time series images (Table 1) and local governmental records, the years of dykes constructed and associated reclamation zones can be effectively identified, producing a historical reclamation map in Figure 3.

From Figure 3, it can be estimated that a total of 5,637 ha of reclaimed lands already existed before 1969. Since 1969, reclamation programs have been continuously practiced, with rapidly growing reclaimed areas (Table 2). For example, a total of 3,698 ha and 4,087 ha were developed in 1976 and in 1996, respectively. From 1969 to 1996, a total of 15,668 ha coastal

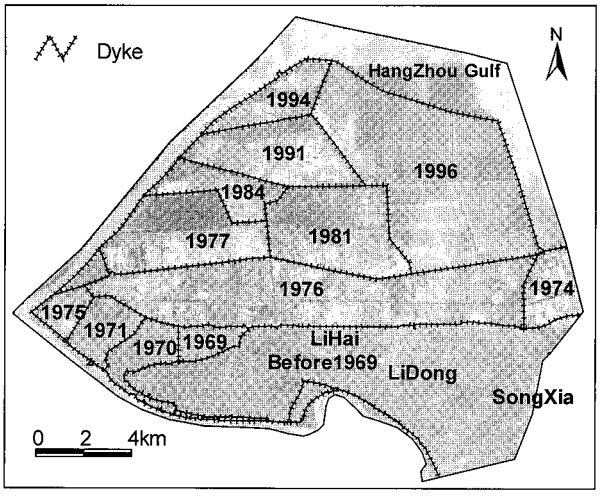

Figure 3. Dykes and reclaimed areas in different years.

lands had been enclosed and reclaimed, almost three times of the reclaimed area before 1969. These reclaimed lands have been used to alleviate the pressure from ever-increasing population and to promote local economic developments.

Complex soil characteristics and a variety of land covers exist for the reclaimed lands. Based on the reclamation years, locations, and sampled land covers, the study area was grouped into six sub-zones: (a) Zone 0, located outside of the reclaimed areas and dominated by tidelands and rivers; (b) Zone 1, reclaimed before 1969; (c) Zone 2, reclaimed between 1969 and 1981; (d) Zone 3, reclaimed between 1981 and 1991; (e)

Table 2. Reclaimed areas in different years

Reclamation years	Before 1969	1969	1970	1971	1974	1975	1976	1977	1981	1984	1991	1994	1996
Reclaimed areas (ha)	5637	284	565	472	542	271	3698	1495	1601	747	1269	637	4087
Cumulative percentage of areas (%)	26	28	30	33	35	36	54	61	68	72	78	81	100

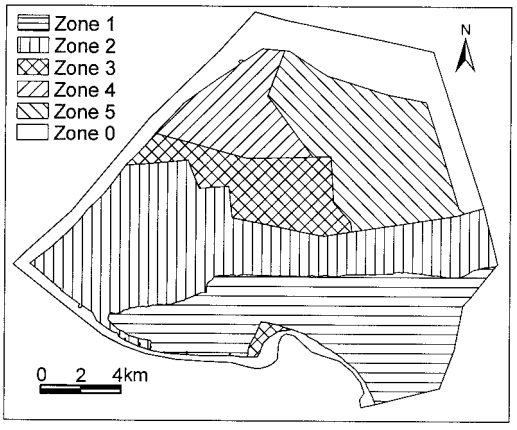

Figure 4. Sub-zones of the study area.

Zone 4, reclaimed between 1991 and 1996; and (f) Zone 5, reclaimed after 1996 (Figure 4). Conducting such a zoning procedure enables subsequent comparisons of different land uses between zones. Also, for individual zones different image classifiers could be employed to reduce the following land-use misclassification because the zoning concept allows a locally adaptive determination of class parameters in the classification, rather than a uniform treatment for an entire study area. For example, it is usually difficult to separate areas with barren saline lands with scattered low-density wildgrass and towns due to their similar spectral reflectance. Because newly reclaimed lands (e.g., Zone 5) are the areas with most likely barren saline soils and early reclaimed areas (e.g., from Zone 1 to Zone 4) would have built-up towns, classification for the zoned areas with distinct land covers can be specifically targeted using desirable methods (Figure 4).

Classification

A modified land-use classification system was proposed with reference to the classic land-cover and land-use classification system from Anderson and others (1976) (Table 3). The modified system is designed for the classification of coastal lands in the study area, although other systems could also be defined applicable to different study regions.

Table 3. A modified land-use classification system

Level I	Level II	Level III
100 Town or built-up	110 Residential	
	120 Industrial or open land	
	130 Road and dyke	
200 Agriculture	210 Cropland	211 Cotton field
		212 Paddy field
		213 Mixed field
	220 Orchard	
300 Forest land		
400 Water	410 River and gulf	
	420 Canal and pond	
	430 Aqua-farm pond	
500 Barren land	510 Tideland	
	520 Saline land with wildgrass	
	530 Non-vegetated saline land	

Before carrying out classification, two main cropping systems are investigated for the study area: (1) cotton, and barley or wheat in cotton fields—a planting period for cotton is from late April (spring) to early November (autumn), and barley or wheat is planted in fallow cotton fields in winter and early spring; and (2) paddy, and rape (*Brassica Napus*) in paddy fields—the planting period for paddy is from early May to late October, and rape is planted in fallow paddy fields in winter and early spring. As crops grow with seasonal and annual phenological cycles, images captured at different seasonal dates can highlight seasonal phenological differences and cropping systems at different seasons could be perceived.

Two classification methods were adopted for different zoned areas (Figure 2). For Zone 0 and Zone 5, an unsupervised ISODATA classifier was conducted with resolution-sharpened images (4 May 2000). From Zone 1 to Zone 4, a supervised maximum likelihood (ML) classifier was applied with derived images from the following two spectral processing methods: Tasseled Cap transformation and vegetation indices. These two methods are often used for spectral feature extraction

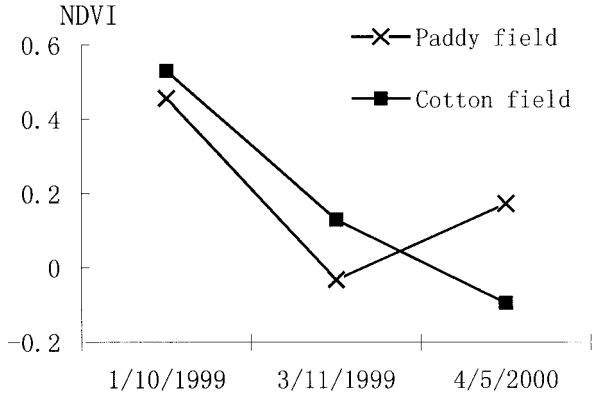

Figure 5. NDVI of paddy and cotton fields at different seasonal dates.

and data reduction with multitemporal images, and their derived images can be very useful for monitoring the characteristics of crops and vegetation (e.g., Richards 1994).

Tasseled Cap transformation is a linear transformation, and the first three features derived from Landsat TM images are known as brightness, greenness, and wetness. These three features, which have physical significance, can typically express 95% or more of the total variability of the original images (Crist and Kauth 1986). In this study, Tasseled Cap transformations were performed with the images at three different dates (1 October 1999, 3 November 1999, 4 May 2000), and for each image the first two features (i.e., brightness and greenness) were extracted.

At wavelengths from 0.63 to 0.69 μm (visible red band) the chlorophyll pigment of healthy green vegetation strongly absorbs sun radiation, and at wavelengths from 0.76 to 0.90 μm (near-infrared band) multiple scattering occurs due to the leaf's internal mesophll structures. Because these two bands are closely related to the amount of vegetation biomass, they are very useful for vegetation discrimination and crop identification (Jensen 1996). In this regard, various vegetation indices, such as a Normalized Difference Vegetation Index (NDVI), are often used. With TM images, NDVI can be calculated by $(NIR_{TM4} - R_{TM3})/(NIR_{TM4} + R_{TM3})$, where NIR_{TM4} and R_{TM3} are the digital number (DN) of TM band 4 (near-infrared band) and band 3 (red band), respectively. For those sampled paddy and cotton fields, their NDVI values were −0.03 and 0.13 from the image dated 3 November 1999, dropping greatly from those with the 1 October 1999 image (Figure 5). These changes reflected the fact that, for the study area, paddy was harvested just before 3 November yet after 1 November, with rare vegetation cover and/or young rapes in paddy fields; from October to November cotton approached harvest period, with decreasing and little green leafs. On the other hand, using the image of 4 May 2000 NDVI values for paddy and cotton fields were 0.17 and −0.1, respectively. These showed different trends in comparison to the NDVI values from the image on 3 November 1999. This is because paddy was planted again with medium-density green coverage early May, while young cotton just planted late April had low-density green leafs (predominantly soil surfaces). Multitemporal images on crops at a growing season and in a leaf-less period can be used to enhance the seasonal phenological differences, thus increase discrimination abilities for various crops. In a sense, from the change of NDVI values images collected at spring and fall dates were particularly useful for suggesting cropping rotation systems and discriminating crop types.

Finally, a total of nine derived images (i.e., brightness, greenness and NDVI at three different dates) were input to the ML classifier for land-use classifications from Zone 1 to Zone 4.

Results

The classified image is shown in Figure 6, and an error matrix for accuracy assessment is shown in Table 4. Reference data are in columns representing ground-truth samples collected by field investigation, and classified land-use classes are in rows. Both user's accuracy and product's accuracy of each land-use type can be calculated. In this study, an overall classification accuracy of 77.8% was achieved. Among all classified land-use types, waters had the highest user's accuracy (97.4%), followed by barren lands and croplands (equal or larger than 80%). However, the user's accuracy for orchards and forest lands were lower, being 74.5% and 62.5%, respectively. Since it is popular to have various family vegetables scattered in vineyards and pear yards, their mixed spectral signatures reduced the classification accuracy for orchards. For many forest lands located along dykes and roads as green ecological belts, their narrow and sometimes fragmentary spatial distributions caused very low classification accuracy. Also, in subtropical regions temporal signatures of most even-green trees are less significant than those of croplands, and this fact partially weakens the approach to correctly classify forest lands.

Table 5 summarizes areas of classified land uses in different sub-zones. Agricultural lands, including croplands and orchards, occupy 44.4% of the whole study area. If aqua-farm ponds and forest lands are included, up to 63% of an entire study area was used for agricul-

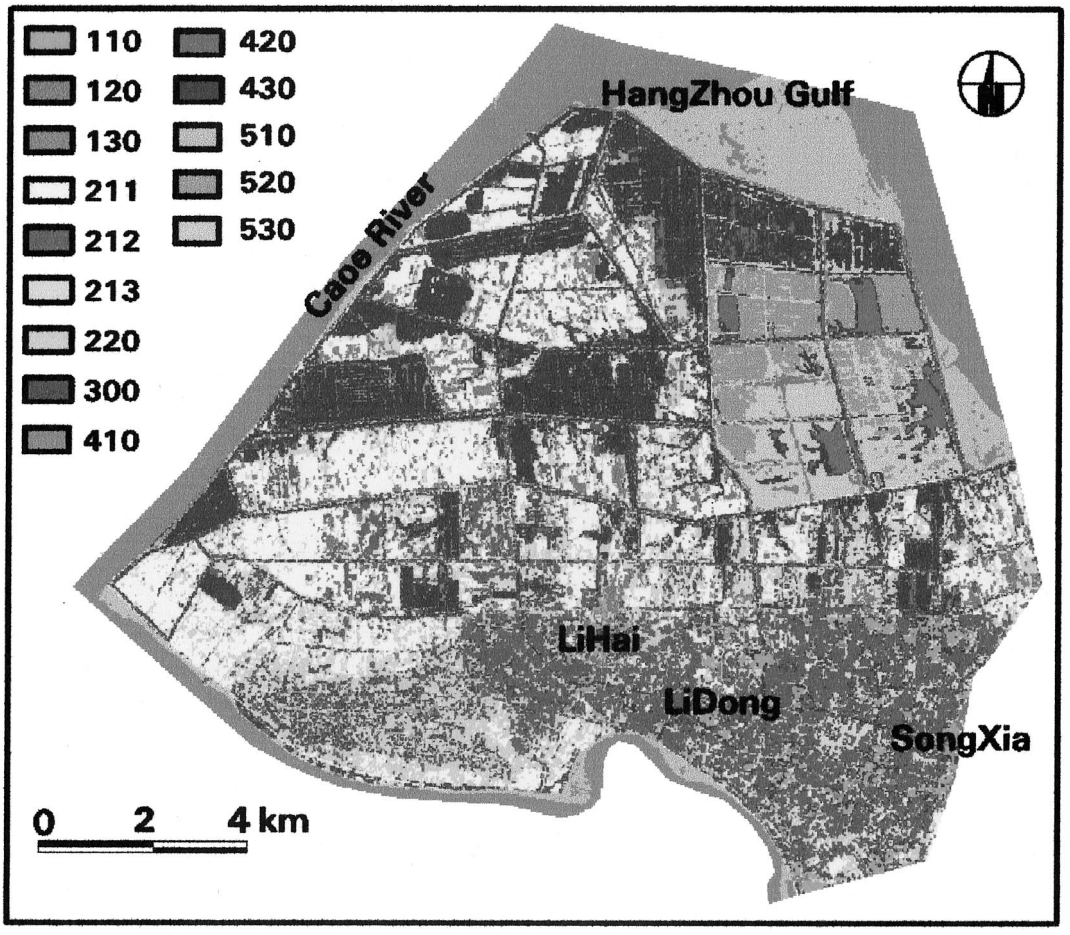

Figure 6. Classified land-use map.

tural production and forest. Figure 7 shows the percentages of cotton fields, paddy fields, orchards, forest lands, aqua-farm ponds, and saline lands with wildgrass, in individual sub-zones. Compositions of land uses in each zone were different and related to the historical reclamation years. For example, Zone 5 (reclaimed in 1996) is dominated by saline lands with wildgrass (29.1%) and aqua-farm ponds (26.7%); Zone 3 (reclaimed between 1981 and 1991) is mainly covered by aqua-farm ponds (30.2%) and cotton fields (20.5%); Zone 1 (reclaimed before 1969) is dominated by paddy fields (35.0%) and orchards (16.4%). Land uses for agricultural production are changing from simple saline lands with wildgrass (Zone 5) to aqua-farm ponds and cotton fields (Zone 4 and Zone 3), to cotton fields and aqua-farm ponds (Zone 2), to paddy fields and orchards (Zone 1) (Table 6).

It is found that the above evolution of land uses resulted from the level of soil salinity in individual zones. Soil analyses indicated that a soil electrical conductivity of saturation extract increased from below 2.0 ds/m in early reclaimed saline lands (Zone 1) to 7.3 ds/m in recently reclaimed saline lands (Zone 5). According to Rhoades and Miyamoto (1990), salinity thresholds for paddy and cotton plantation are 3.0 ds/m and 7.7 ds/m, respectively. Therefore, paddy cannot be planted in lands with high salinity levels, such as Zone 5. In fact, for the study area a large portion of paddy plantation was in Zone 1, which was reclaimed for 30 years. An average salinity level in Zone 4 was 3.4 ds/m, suitable for cotton plantation. Due to the higher levels of soil salinity and low cultivation yield in newly reclaimed zones, farmers tend to develop aqua-farm ponds in Zone 5, Zone 4, and Zone 3 for better economic returns.

Discussion

Although a series of vegetation-specific feature images derived from multi-temporal images were used for

Table 4. An error matrix with the classified land use map and reference data

	Reference data									
Land uses	211	212	213	220	300	430	520	530	Total	User's accuracy (%)
Classified data										
211	56	5	6	1	1	0	1	0	70	80.0
212	4	54	4	1	0	0	0	0	63	85.7
213	5	3	63	3	3	1	0	0	78	80.8
220	2	1	4	35	5	0	0	0	47	74.5
300	1	1	4	6	20	0	0	0	32	62.5
430	0	0	0	0	0	38	0	1	39	97.4
520	1	0	1	0	1	1	23	1	28	82.1
530	0	0	0	0	0	3	1	27	31	87.1
Others[a]	2	1	2	6	3	2	0	2	18	—
Total	71	65	84	52	33	45	25	31	406	
Producer's Accuracy (%)	80.3	83.1	75.0	67.3	60.1	84.4	92.0	87.1	—	Overall accuracy = 77.8%

[a]Others include towns or built-up, rivers and gulfs, canals and ponds, and tidelands.

Table 5. Areas of different land uses of sub-zones and an entire study area (ha)

Land use type	Zone 0	Zone 1	Zone 2	Zone 3	Zone 4	Zone 5	Entire area
110 Residential	—	514.21	54.73	29.81	—	—	598.76
120 Industrial or open land	—	171.14	327.63	168.11	133.71	53.37	853.96
130 Road and dyke	—	10.95	300.65	162.25	112.89	258.59	845.33
211 Cotton field	—	293.12	2157.23	484.01	601.79	88.65	3624.80
212 Paddy field	—	2020.88	488.41	78.68	32.55	16.91	2637.42
213 Mixed field	—	1054.91	1334.94	361.74	206.72	62.46	3020.76
220 Orchard	—	945.44	989.52	176.91	108.00	66.76	2286.63
300 Forest land	—	533.56	466.22	102.82	49.95	27.17	1179.73
410 River and gulf	2919.07	—	—	—	—	—	2919.07
420 Canal and pond	—	103.12	242.59	85.72	60.89	438.94	931.26
430 Aqua-farm pond	—	128.24	1082.77	715.26	620.26	1121.77	3668.30
510 Tideland	1427.41	—	—	—	—	—	1427.41
520 Saline land with wildgrass	—	—	—	—	—	847.14	847.14
530 Non-vegetated saline land	—	—	—	—	—	1221.05	1221.05
Total	4346.48	5775.57	7444.68	2365.32	1926.75	4202.81	26061.61

the supervised land-use classification, a moderate accuracy of 77.8% was achieved. This is in part caused by the small patchy structures of underlying lands, which are spatially over-fragmented. According to Statistic Bureau of Zhejiang Province (1999), in the study area each household has an overage of 0.17 ha farmlands, and the average size of each land plot is 0.097 ha. Adjacency two plots are usually separated by low banks of earth and/or irrigation ditches (Hu 1997). Considering that the pixel area of TM multispectral imagery with a spatial resolution of 30 m is 0.09 ha, a small land plot with an area less than a pixel could not be well represented in the images, and are infeasible to be classified. Many pixels with mixed land covers contribute to the difficulty of producing good classification accuracy.

Nevertheless, time series Landsat TM images for detecting coastal land uses and monitoring their changes are of practical use. For example, the new Landsat-7 ETM+ imagery has its advantages with an acceptable cost, a 15 m resolution panchromatic band, multispectral bands, and relatively short revisit period (16 days). An ETM+ scene costs US $610, covering an area of 31,450 sq km. By comparison, an aerial photograph at a 1:10,000 scale would cost US $30 per sq km, and IKONOS GEO images would cost US $35 per sq km in a panchromatic band with 1 m resolution, or multispectral bands with 4 m resolution. In spite of the very high spatial resolution of these images, higher costs hinder their wider agricultural applications, particularly when a large area is concerned.

Landsat images can be used to produce maps with large scales, either in a direct printing output or during land-use mapping. It is reported that a printed Landsat image with a printing resolution of 6 pixels per milli-

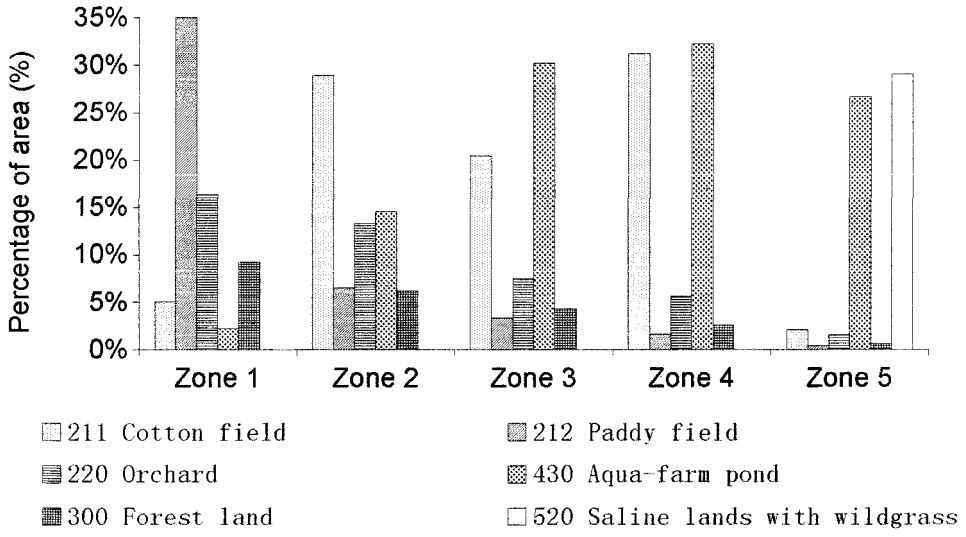

Figure 7. Percentages of main land uses in different sub-zones.

Table 6. Agricultural land-use changes between sub-zones

Sub-zone	Zone 5	Zone 4	Zone 3	Zone 2	Zone 1
Main land uses (area percentage > 10%)	Saline land with wildgrass Aqua-farm pond	Aqua-farm pond Cotton field	Aqua-farm pond Cotton field	Cotton field Aqua-farm pond Orchard	Paddy field Orchard

meter can provide an acceptable quality for image features (Light 1990). Using the printing criterion of 5 pixels per millimeter adopted in China, a resolution-sharpened ETM+ imagery (i.e., with a resolution of 15 m) should produce a printed photographic sheet at a scale of 1:90,000. During the land-use mapping, classified images are subject to a raster-to-vector conversion and spatial generalizations dependent upon a minimum mapping unit (MMU), and areas smaller than the MMU are removed. The area of a typical MMU for land-use mapping at a 1:50,000-scale in China is 0.25 ha (Shen 1991), and therefore resolution-sharpened ETM+ imagery with a pixel area of 0.0215 ha can meet the requirement of land-use mapping at a scale of 1:50,000. This scale is commonly used for producing base maps (e.g., land uses) in agricultural applications in China.

This study takes advantages of the available Landsat images, particularly the recent Landsat-7 ETM+ images. The acquisition of satellite-based remotely sensed images for subtropical coastal regions in China is often hampered by adverse atmospheric conditions, such as heavy cloud covers. According to historical climatic records of Zhejiang Province between 1960 and 1990, the average number of dates each year with cloud covers less than 20% is 59. With the revisit cycle of 16 days for Landsat, only three or four images with an acceptable quality can be received each year for the study area; in over-raining years (e.g., 1996), only one valid image can be acquired.

Conclusions

Coastal lands reclaimed in the past are characterized by substantial variations in soil compositions, and a variety of land covers. Obtaining synoptic, up-to-date, and reliable spatial information of coastal land uses and their dynamic changes, combined with holistic and effective management measures, is critical to the sustainable development of coastal regions. In this study, multi-temporal Landsat images offered a unique opportunity to detect coastal land-use and monitor their changes in a cost-effective way. Not only do the time series images facilitate the delineation of the expanding areas of reclaimed coastal lands over the years, but they enable the classification of detailed land uses. It was found that the land uses in different historically-reclaimed zones are determined by soil salinity levels. While significant coastal tidelands have been reclaimed for cultivation in the past 30 years to alleviate the

pressure from the population growth and promote local economic developments, the impact of reclamation programs on the marine ecology in the tidelands of Hangzhou Gulf deserves attention. Future research on tidelands-sea interactions and their changes, with remotely sensed images and field investigations, would be pursued.

Acknowledgments

This study was supported by the National Natural Science Foundation of China (No. 40001008), the Natural Science Foundation of Zhejiang Province (No. 499043), and the German Federal Ministry for Research and Education under grant AZ39742 (BMBF). The authors would like to thank Dr. Keping Chen, Natural Hazards Research Centre, Macquarie University, Australia for his valuable comments. Constructive suggestions from the two reviewers are highly appreciated.

Literature Cited

Anderson, J. R., E. E. Hardy, J. T. Roach, and R. E. Witmer. 1976. A land use and land cover classification system for use with remote sensor data. USGS Professional Paper 964

Crist, E. P., and R. J. Kauth. 1986. The Tasseled Cap demystified. *Photogrammetric Engineering and Remote Sensing* 52(1):81–86

Dwivedi, R. S., and B. R. M. Rao. 1992. The selection of the best possible Landsat TM band combination for delineating salt-affected soils. *International Journal of Remote Sensing* 13(11):2051–2058

El-Khattib, H. M., N. M. El-Mowelhi, and F. Hawela. 1996. Monitoring land cover of the desert fringes of the eastern Nile Delta, Egypt. Pages 1756–1758 *in* Proceedings of IGARSS'96, Vol. 3, IEEE, Lincoln, Nebraska, 27–31 May 1996

Goetz, S. J., S. D. Prince, M. M. Thawley, A. J. Smith, R. Wright, and M. Weiner. 2000. Application of multi-temporal land cover information in the mid-Atlantic region: A RESAC initiative. Pages 357–359 *in* Proceedings of IGARSS'2000, Vol. 3, IEEE, Honolulu, Hawaii, 24–28 July 2000

ERDAS, Inc. 1999. ERADS field guide. Atlanta, GA

Hill, J., and J. Megier. 1988. Regional land cover and agricultural area statistics and mapping in the Department Ardeche, France, by use of Thematic Mapper data. *International Journal of Remote Sensing* 9(10):1573–1595

Hill, J., and J. Megier. 1989. The use of multi-temporal TM tasseled cap features for land use mapping in European marginal areas an operational approach. Pages 798–801 *in* Proceedings of IGARSS'89, Vol. 2, IEEE, Vancouver, 10–14 July 1989

Hu, W. 1997. Household land tenure reform in China: Its impact on farming land use and agro-environment. *Land Use Policy* 14(3):175–186

Jensen, J. R. 1996. Introductory digital image processing: A remote sensing perspective, (2 ed.). Prentice Hall, Upper Saddle River, NJ

Kalra, N. K., and D. C. Joshi. 1996. Potentiality of Landsat, SPOT and IRS satellite imagery for recognition of salt affected soils in Indian arid zone. *International Journal of Remote Sensing* 17(15):3001–3014

Light, D. L. 1990. Characteristics of remote sensors for mapping and earth science applications. *Photogrammetric Engineering and Remote Sensing* 56(12):1613–1623

Mumby, P. J., D. A. Gray, J. Gibson, and P. S. Raines. 1995. Geographic Information Systems: A tool for integrated coastal zone management in Belize. *Coastal Management* 23(2):111–121

Pax-Lenney, M., and C. E. Woodcock. 1997. Monitoring agricultural lands in Egypt with multi-temporal Landsat TM imagery: How many images are needed? *Remote Sensing of Environment* 59(3):522–529

Peng, W. L. 1998. Synthetic analysis for extracting information on soil salinity using remote sensing and GIS: A case study of Yanggao Basin in China. *Environmental Management* 22(1):153–159

Rhoades, J. D., and S. Miyamoto. 1990. Testing soils for salinity and sodicity. Pages 299–366 *in* R. L. Westerman (ed.) Soil testing and plant analysis, Soil Science Society of American, Madison, WI

Richards, J. A. 1994. Remote sensing digital image analysis: An introduction (2 ed.), Springer-Verlag, Berlin.

Salem, B. B., A. El-cibahy, and M. El-raey. 1995. Detection of land cover classes in agro-ecosystems of northern Egypt by remote sensing. *International Journal of Remote Sensing* 16(14):2581–2594

Shen, X. 1991. Preliminary study on land use mapping. Pages 114–121 *in* L. Ke and F. Suxing (eds.), Proceedings of Agricultural Mapping, Science Press, Beijing

Statistic Bureau of Zhejiang Province. 1999. Zhejiang statistical yearbook 1998. Statistic Bureau of Zhejiang Province, Hangzhou (in Chinese)

Wheeler, J. R., C. Jarvis, A. J. B. Mitchell, R. B. King, and R. J. White. 1988. Evaluation of Landsat and Spot imagery for agricultural land use planning in less developed country. Pages 471–472 *in* Proceedings of IGARSS'88, Vol. 1, IEEE, Edinburgh, 12–16 September 1988